Shock formation at the magnetic collimation of relativistic jets

S. Bogovalov[1] and K. Tsinganos[2]⋆

[1]*Moscow Engineering Physics Institute, Moscow 11549, Russia*
[2]*IASA and Department of Physics, University of Athens, Panepistimiopolis Zografos, 157 84 Greece*

ABSTRACT

If the observed relativistic plasma outflows in astrophysical jets are magnetically collimated and a single-component model is adopted, consisting of a wind-type outflow from a central object, then a problem arises with the inefficiency of magnetic self-collimation to collimate a sizeable portion of the mass and magnetic fluxes in the relativistic outflow from the central object. To solve this dilemma, we have applied the mechanism of magnetic collimation to a two-component model consisting of a relativistic wind-type outflow from a central source and a non-relativistic wind from a surrounding disc. By employing a numerical code for a direct numerical solution of the steady-state problem in the zone of super-fast magnetized flow, which allows us to perform a determination of the flow with shocks, it is shown that in this two-component model it is possible to collimate into cylindrical jets all the mass and magnetic fluxes that are available from the central source. In addition, it is shown that the collimation of the plasma in this system is usually accompanied by the formation of oblique shock fronts. The non-relativistic disc-wind not only plays the role of the jet collimator, but it also induces the formation of shocks as it collides with the initially radial inner relativistic wind and also as the outflow is reflected by the system axis. Another interesting feature of this process of magnetic collimation is a sequence of damped oscillations in the width of the jet.

Key words: MHD – stars: mass-loss – pulsars: general – stars: winds, outflows – ISM: jets and outflows – galaxies: jets.

1 INTRODUCTION

Observations from various classes of astrophysical sources indicate the existence of collimated relativistic outflows in the form of jets (Ferrari 1998; Heyvaerts & Norman 2003). Thus, in active galactic nuclei (AGN) and quasars, the inferred bulk Lorentz factors are $\gamma = 5$–10 (Biretta, Sparks & Macchetto 1999; Cramphorn, Sazonov & Sunyaev 2004), while in galactic superluminal sources $\gamma \sim 2$ (Mirabel & Rodríguez 1999). The prevailing view is that the toroidal magnetic field generated by the rotation of the source spontaneously collimates part of the outflow around the axis of rotation (Bisnovatyi-Kogan & Ruzmaikin 1976; Blandford 1976; Lovelace 1976; Heyvaerts & Norman 1989, 2003; Chiueh, Li & Begelman 1991; Sauty & Tsinganos 1994; Bogovalov 1995; Vlahakis & Tsinganos 1998, 1999; Vlahakis et al. 2000; Gabuzda, Eammon & Cronin 2004). Nevertheless, to calculate the fraction of the collimated fluxes or the distance where the collimated outflow is formed, one needs direct numerical simulations for every specific case (Kudoh, Matsumoto & Shibata 1998; Krasnopolsky, Li & Blandford 1999; Ustyugova et al. 1999). In Bogovalov & Tsinganos (1999, hereafter BT99) and Tsinganos & Bogovalov (2000, hereafter TB00), it was found

that the fraction of the cylindrically collimated part of the wind is of the order of 1 per cent of the total mass and magnetic fluxes of the initially (i.e. before rotation sets in) uncollimated wind from the source, when the source rotates uniformly. Recently, the same conclusion about the collimation of an unacceptably small percentage of cylindrically collimated flux of a wind from a disc has been confirmed by Krasnopolsky, Li & Blandford (2003). However, observations and theoretical arguments indicate that a higher percentage of the mass and magnetic flux should be collimated inside the jet.

One of the simplest resolutions of this contradiction for the case of relativistic outflows has been proposed in Tsinganos & Bogovalov (2002, hereafter TB02). In this paper we use a simplified model to demonstrate that the mechanism of magnetic collimation of outflows may provide collimation of a remarkable fraction of the total magnetic and relativistic mass flux from a source provided that the system consists of two components: an initially uncollimated relativistic plasma from the central source and a non-relativistic wind from the surrounding disc. In the particular case studied in TB02, the toroidal magnetic field in the wind from the central source was negligible by assuming that the angular velocity of the central source is negligible. Under this condition, the disc-wind plays the role of the collimator of all the relativistic outflow from the central source. For the relativistic jet we were able to obtain a steady-state

⋆E-mail: tsingan@phys.uoa.gr

solution having a Lorentz factor $\gamma = 5$. The total magnetic and mass flux from the central source of the relativistic outflow was about 30 per cent of the total fluxes from our system. It is important that all (100 per cent) the mass from the central source is collimated into a relativistic jet. In the process of numerical modelling in TB02, it was found that the collimation of the central source relativistic wind is accompanied by the formation of oblique shock waves in the flow. However, the numerical code that we used in TB02 was created in order to model continuous flows. Therefore, we were unable to perform a detailed investigation of the process of collimation for a variety of parameters. To meet this need, in the present work we have modified the numerical code, which allows us now to consider the flow with the shock fronts and to perform the numerical simulation of the process of collimation accompanied by the formation of shocks.

2 THE MODEL

The idea that jet formation requires the existence of two components in the outflow, one originating at the central source and the other in the accretion disc, has been already discussed in the literature in the context of AGN (Sol, Pelletier & Asseo 1989; Pelletier et al. 1996) or young stellar objects (Ferreira, Pelletier & Apple 2000). In models proposed to explain the time-dependent quasi-periodic oscillation in accretion discs around black holes, the disc is assumed to have a Shakura–Sunyaev (SS; Shakura & Sunayev 1973) radiatively efficient external part and a radiatively inefficient inner part where an advection dominated accretion flow (ADAF) exists. The transition region between the SS disc and the ADAF is found to be highly variable (Gracia et al. 2003). In such models it is assumed that a radial outflow originates at the corona of the ADAF part of the disc and a disc-wind from the SS part. Also, observations show that AGN jets are slowly collimated across parsec scales from the central engine. This scale is significantly larger than that of the black hole, suggesting that the accretion disc plays an important role in the initial jet collimation. For example, observations of the M87 jet (Biretta, Junor & Livio 2002) show that the initial opening angle of the jet is about $60°$ in the smallest physical scales yet probed for M87 (~ 0.01 pc), while later the opening angle becomes a few degrees. This is consistent with the picture of poloidal collimation of the jet by the magnetic field of the disc (Spruit 1994; Livio 1999). Recently, this approach seems that it may become more and more related to the physics of cosmic gamma-ray bursts (GRBs), wherein models have been proposed where the main engine of the GRB is the central black hole surrounded by a massive accretion torus.

According to this picture, in the model we adopt, the outflow has two components: a radially expanding outflow with a uniform speed $v_{\rm jet}$ having its origin at the central source and a non-relativistic outflow at the accretion disc, which initially expands radially as well with speed $v_{\rm disc}$. We assume in addition that the wind from the disc is non-relativistic because relativistic winds are poorly collimated by magnetic stresses. The total poloidal magnetic field initially has a monopole-like structure. The inner relativistic wind originates at the central source and the base of the outflow for this outflow component is taken to be spherical. On the other hand, the accretion disc is attached to the spherical central base as a slab (Fig. 1). The thickness of this slab defines the magnetic and mass flux from the disc. For simplicity, the radius of the disc is assumed to be twice as large as the radius of the base of the central flow component. At this stage of our investigation, we do not care about a close correspon-
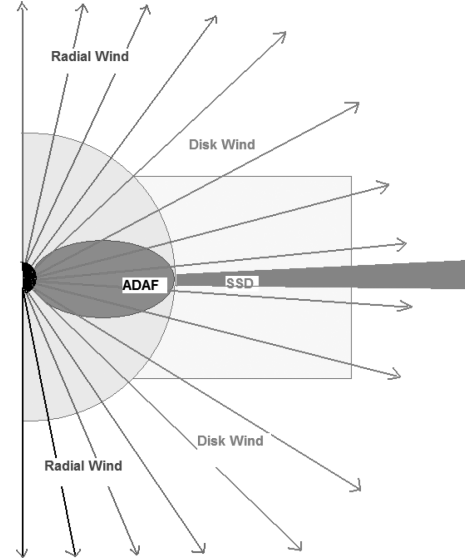

Figure 1. Sketch of the initial ($t = 0$) state of the two-component outflow model. A central relativistic radial outflow originates in the hot corona surrounding an ADAF while a non-relativistic rotating disc-wind originates in a surrounding SS disc. For simplicity, the launching boundary of the inner outflow from the ADAF corona is taken at a spherical surface surrounding the ADAF while the boundary of the SSD is on a rectangular slab attached to the spherical surface around the ADAF. Thin solid lines indicate lines of the poloidal magnetic field.
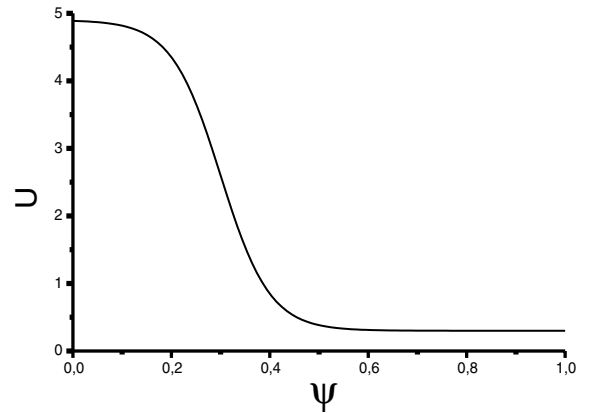
Figure 2. Assumed initial ($t = 0$) state of the two-component outflow model with a central relativistic radial outflow originating in the hot corona surrounding the central object and ADAF and a non-relativistic rotating disc-wind originating in a surrounding SS disc.

dence of the parameters of the model to some specific astrophysical object, because our purpose here is to demonstrate the possibility to collimate relativistic winds, to investigate the formation of shocks in the flow and to define the conditions under which this may take place. For the same reason, we omit here gravity and the thermal pressure of the plasma at the base, which is thus assumed to be initially cold. Of course, in the post-shock region the plasma is heated. We are mainly interested in the electromagnetic stresses acting on the wind.

We specify the Lorentz factor of the relativistic plasma ejected by the central source to be $\gamma_{\rm jet} = 5$, $U_{\rm jet} = 4.9$ and $v_{\rm jet} = 0.97979c$. On the other hand, the disc-wind is assumed to be non-relativistic
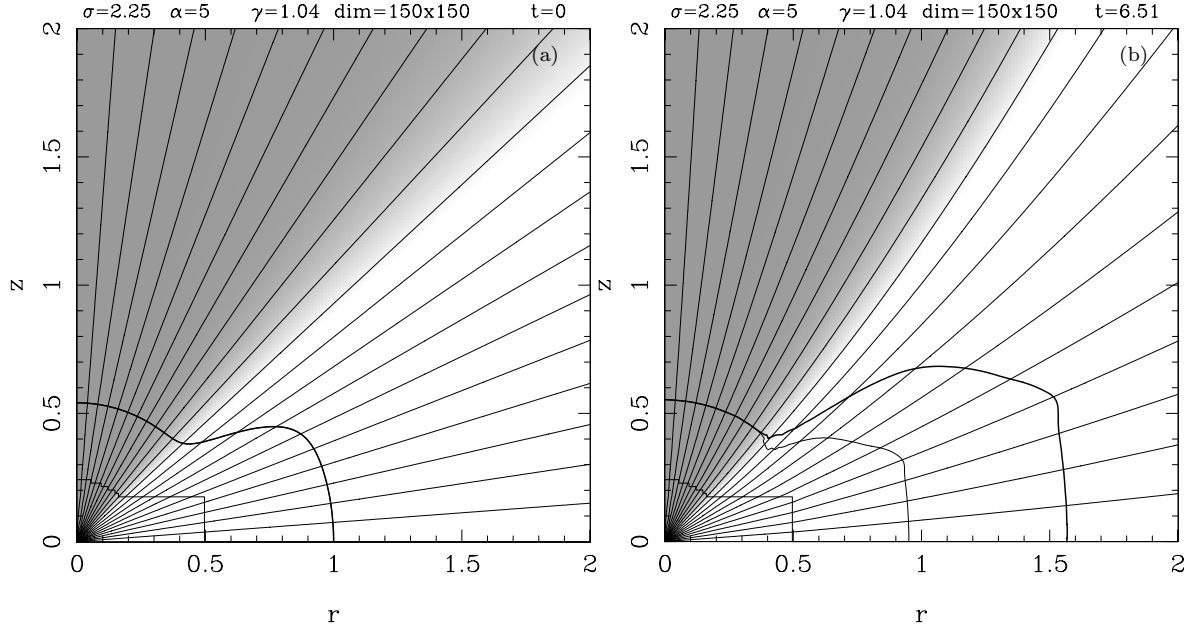
Figure 3. Initial non-rotating monopole magnetic field of the two-component model with a relativistic (non-relativistic) flow speed v_{jet} (v_{disc}) along the radial field lines is shown in the left panel. Thin solid lines indicate lines of the poloidal magnetic field with 20 lines plotted at equal intervals of the separation meridional angle in the initial magnetic field. The shaded (non-shaded) area corresponds to the relativistic wind (non-relativistic disc-wind). The disc-wind provides 70 per cent of the fluxes ($\psi_{disc} = 1 - \psi_{jet} = 0.7$). For comparison, the solution of the problem in the nearest zone is shown in the right panel. The thick solid line indicates the fast mode MHD surface while the thinner line shows the Alfvén surface. The values of the parameters $\sigma = 2.25$ and $\alpha = 5$ refer to the inner edge of the non-relativistic outflow from the disc.

with parameters $v_{disc} = 0.288\,c$, $U_{disc} = 0.3$ and $\gamma_{disc} = 1.044$. This velocity is already small enough to reduce the decollimating effect of the electric field and, on the other hand, it is still not too small compared to the velocity of the wind from the central source to provide strong gradients in the flow which might easily destroy the solution. To avoid strong gradients in the velocity and density, the initial values of these variables are smoothed with a function of the form (Fig. 2)

$$U(\psi) = \frac{(U_{jet} - U_{disc})}{1 + \exp[(\psi - \psi_{jet})/0.05]} + U_{disc}, \tag{1}$$

where U_{jet} is the four-velocity of the plasma ejected from the central source, U_{disc} is the four-velocity of the plasma ejected from the disc and the parameter ψ_{jet} defines the fraction of the magnetic field flux in the jet. All the rest of the magnetic and mass flux originates at the central source. The density increases with the polar angle as we move towards the disc and is taken to keep the mass flux ρU independent of the poloidal magnetic flux ψ and to vary with the velocity such that the Alfvénic radius of the non-relativistic wind emanating from the inner edge of the disc is twice the initial Alfvénic radius of the relativistic flow from the central source. The angular velocity changes smoothly at the region between the central object and the disc from zero to a specified value. Inside the disc, the angular velocity of the disc rotation ω is taken such that $\omega \sim r^{-\delta}$. For $\delta = 3/2$ we have the familiar Keplerian rotation law. The total magnetic flux from the source is normalized to unity at the equator.

For the convenience of the reader, here we recall that all geometrical parameters are expressed in units of the radius of the coinciding initial fast mode and Alfvén surfaces at the equator. The flow is described by the parameters α, σ and ψ_{jet}. The parameter σ is defined

as $\sigma = (R_f/R_1)^2$, where R_f is the initial radius of the fast mode surface (i.e. before rotation of the disc starts), R_1 is the radius of the light cylinder and $\alpha = \sqrt{\sigma}/U_{disc}$, where U_{disc} is the initial four-velocity of the plasma at the inner edge of the disc. The parameter σ approximately equals the ratio of the Poynting and kinetic fluxes. In the case of uniform rotation and uniform flow, these parameters describe the total flow. In our case of latitudinally non-uniform rotation and non-uniform flow, these parameters correspond to the field line leaving the inner edge of the accretion disc. The initial configuration in the nearest zone is shown in the left panel of Fig. 3.

3 METHOD OF SOLUTION

To obtain the steady-state solution of the problem in a wide range of scales, from distances compared to the dimension of the central source up to much larger distances, we used a combination of two methods. A more detailed discussion of these methods is given in BT99.

In our approach, the steady-state solution in the nearest zone, which contains the relevant MHD critical surfaces and where the governing partial differential equations are of mixed elliptic/hyperbolic type, is obtained by using a relaxation method, as in several other studies (cf. Ouyed & Pudritz 1997; Krasnopolsky, Li & Blandford 1999; Ustyugova et al. 1999). We use the same software that has been used in BT99, except for a simple linear interpolation of the variables in the cells, which is here replaced by a van Leer (1977) interpolation scheme in the code for the time-dependent simulation. This modification allows us to reduce strongly the usual Lax–Wendroff artificial oscillations present in our previous works.

In the second step, the solution in the far zone is obtained by extending to large distances the solution obtained in the nearest zone.

This ability to extend the inner zone solution is based on the fact that the outflow in the far zone is already super-fast magnetosonic. Therefore, the problem can be treated as an initial value Cauchy-type problem with the initial values taken on an arbitrary surface located at the base of the far zone. The initial values on this surface are taken from the solution of the problem in the nearest zone. Because later we shall focus more on the solution in the far zone, the method of the solution will be only briefly outlined here for the convenience of the reader.

The problem in the far zone is solved in an orthogonal curvilinear system of coordinates denoted by ψ and η. This system of coordinates has a rather simple physical meaning. The variable ψ in the axisymmetric flow denotes the flux function and gives the poloidal magnetic field B_p as

$$\boldsymbol{B}_p = \frac{\nabla\psi \times \hat{\boldsymbol{\varphi}}}{r}, \tag{2}$$

where $\hat{\varphi}$ is the unit vector in the azimuthal direction and r is the distance from the axis in cylindrical coordinates (z, r, φ). A geometrical interval in the curvilinear system of the coordinates ψ, η and φ can be expressed as

$$(\mathrm{d}\boldsymbol{r})^2 = g_\psi^2 \, \mathrm{d}\psi^2 + g_\eta^2 \, \mathrm{d}\eta^2 + r^2 \, \mathrm{d}\varphi^2, \tag{3}$$

where g_ψ and g_η are the corresponding line elements, or components, of the metric tensor.

The unknown variables here are $z(\eta, \psi)$ and $r(\eta, \psi)$. The metric coefficient g_η can be obtained from the transfield equation (BT99)

$$g_\eta = \exp\left[\int_0^\psi G(\eta, \psi) \, \mathrm{d}\psi \right], \tag{4}$$

where

$$G(\eta, \psi) = \left[\frac{\partial}{\partial\psi} \left(\frac{B^2 - E^2}{8\pi} + P \right) \right.$$
$$\left. - \frac{1}{r} \frac{\partial r}{\partial\psi} \left(U_\varphi v_\varphi c\rho - \frac{B_\varphi^2 - E^2}{4\pi} \right) \right]$$
$$\times \left(U_p v_p c\rho - \frac{B_p^2 - E^2}{4\pi} \right)^{-1}. \tag{5}$$

Here, the four-velocity includes the inertial term produced by the finite temperature, $U = \gamma (v/c)(e + p)$, where e and p are the internal energy and pressure per particle in mc^2 units.

The lower limit of the integration in equation (4) is chosen to be 0 such that the coordinate η is uniquely defined. In this way η coincides with the coordinate z where a surface of constant η crosses the axis of rotation.

The metric coefficient g_ψ can be obtained from equation (2) in terms of the magnitude of the poloidal magnetic field

$$g_\psi = \frac{1}{r B_p}. \tag{6}$$

The equations for r and z are then

$$r_\eta = -\frac{z_\psi g_\eta}{g_\psi}, \qquad z_\eta = \frac{r_\psi g_\eta}{g_\psi}, \tag{7}$$

with g_η calculated by equation (4). Here $r_\eta = \partial r/\partial\eta$, $z_\eta = \partial z/\partial\eta$, $r_\psi = \partial r/\partial\psi$, $z_\psi = \partial z/\partial\psi$. For the numerical solution of the system of equations (7) the two-step Lax–Wendroff method was used, as in our previous work. However, this method appeared unable to resolve the problem with shock formation in the flow. In the present work, we modified the method of the solution of the equations. For the calculation of the variables on the faces of the cells, the Godunov (1959) method has been used.

## 4 RESULTS ON SHOCK FORMATION

For a system consisting of a spherical central source, to which a rectangular disc is attached with a radius twice larger than the radius of the central source, as sketched in Fig. 1, the steady-state solution in the nearest zone is shown in Fig. 3(b). Because we have assumed that only the disc rotates, poloidal electric currents are generated along the field lines which are rooted on this disc. The first notable features from Fig. 3(b) are (i) the collimation of the initially radial disc-wind towards the axis of rotation with a subsequent compression of the wind from the central source and (ii) the splitting of the Alfvén and fast MHD surfaces in the lines which are rooted in the rotating disc.

The MHD collimation of the two-component outflow is evident in the far zone solution displayed in Fig. 4(a), i.e. up to distances $R \approx 10^5 \, R_f$. The total flux from the axis $\theta = 0$ to the equator at $\theta = \pi/2$ is normalized to 1, and 100 lines are plotted in flux intervals $\delta\psi = 10^{-2}$. The initial monopole magnetic field has a flux distribution, $\psi(R, \theta) = (1 - \cos\theta)/R$, such that $R\delta\psi = \sin\theta\delta\theta$, where θ is the polar angle. Hence, in Fig. 4(b) a rather small fraction of the flux is concentrated around the axis. By comparing this initial configuration (Fig. 4b) with the final configuration (Fig. 4a), a rather dramatic concentration of the flux around the axis of the jet may be seen.

Fig. 5 shows the distribution of the various pressures along the surface of constant η, which crosses the z-axis at the distance of $10^5 \, R_f$. The total pressure is uniform across the jet around the outflow's axis, $0 < \psi \leqslant 0.1$; in fact, the pressure there is dominated by the thermal pressure of the heated post-shock plasma, although initially the plasma was cold. At an intermediate layer (e.g. $0.1 < \psi \leqslant 0.3$), the compression of the flux around the core of the jet contributes a dominant poloidal magnetic field pressure. With the toroidal field peaked around $\psi = 0.3$, it is now the turn of the pressure associated with the toroidal field to dominate the total pressure. Further away at $\psi \geqslant 0.3$, all pressure contributions have dropped to negligible values. Nevertheless, equilibrium is maintained by the tension of the surrounding magnetic field. It is worth noting that all magnetic flux that emerges from the central source is concentrated in the jet. This means that, as expected, all the matter flux from the central source is collimated into the jet and thus the model under consideration can be applied to the modelling of observed jets from astrophysical objects.

To understand the structure of the jet and how it is finally formed, it is necessary to consider the process of the collimation in some more detail. Fig. 6 shows schematically the interaction of the two components of the outflow which form the jet and the accompanying shock. The collimation of the relativistic outflow from the central source is performed by the tension of the toroidal magnetic field, which is generated by the rotating disc-wind. This wind which compresses the outflow from the central source in general induces the formation of the oblique shock (1) and a weak discontinuity (2), although for a special choice of the parameters the formation of shock (1) can be avoided (TB02). After the compression of the flow towards the axis, a reflection shock wave (3) may also be formed.

Our numerical simulation shows the gradual formation of the shock and the subsequent collimation of the outflow as follows.
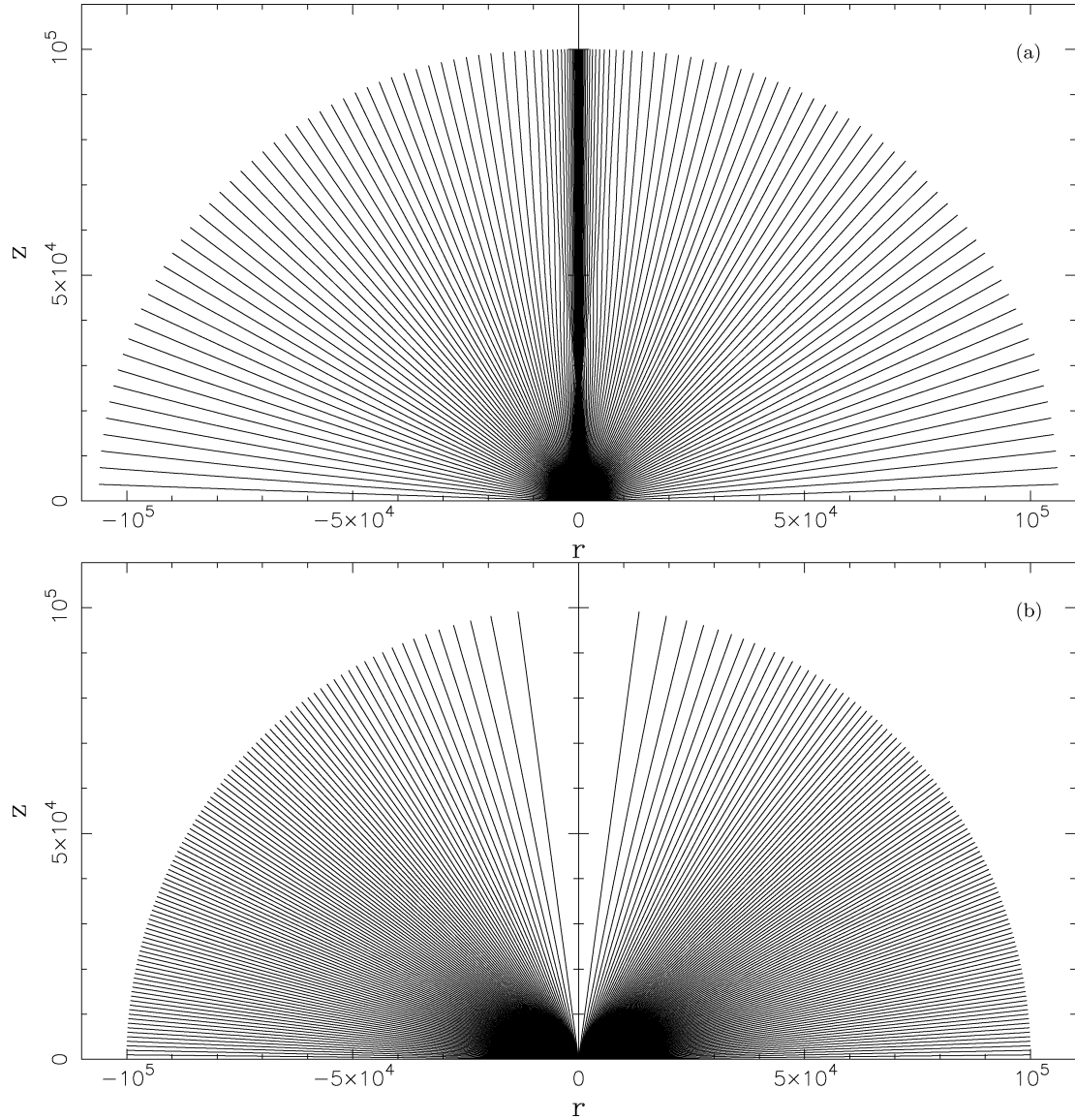
Figure 4. (a) The poloidal magnetic field lines of the outflow shown in Fig. 3 are plotted in the far zone and for intervals of equal magnetic flux $\Delta \Phi = 10^{-2}$ for a total normalized flux $\Phi = 1$. A notable feature in this case is the compression of the part of the inner relativistic flow from the central source into a thin layer of enhanced poloidal magnetic field. A shock wave is formed at the inner part of this layer. The magnetic flux between adjacent field lines is constant. For comparison, the original uncollimated monopole magnetosphere is shown in (b).

First, Fig. 7 shows the formation of the shock when the relativistic flow is compressed by the wind from the disc. The shock is first formed at a distance $R \approx 100 R_f$ from the source. Initially, close to the source the post-shock pressure is mainly provided by the pressure of the poloidal magnetic field, because there the poloidal magnetic field is still sufficiently strong. Thus, a layer of enhanced poloidal magnetic field is formed in the flow and this may be seen in Fig. 7 as a black ribbon. In Fig. 8(a), which shows the pressure distribution along a surface of constant η crossing the z-axis at the distance $412 R_f$, shock (1) has not hit the z-axis yet, and the thermal pressure plays a dominant role in the post-shock region. The further away from the source we move, the weaker the poloidal magnetic field becomes. Starting from some distance (in this case somewhere around $400 R_f$), the poloidal magnetic field is no longer able to provide the needed pressure in the post-shock

region. This role is now taken by the gas pressure, i.e. the total post-shock pressure becomes mainly of thermal origin, as shown in Fig. 8(a).

The shock front reaches the z-axis at a distance $z \approx 2000 R_f$. The pressure distribution corresponding approximately to this situation is shown in Fig. 8(b). Contrary to what was expected, the reflecting shock front (3) has not been formed yet at the interaction of shock (1) with the z-axis. In Fig. 8(b) the shock has reached the z-axis and the pressure is slightly increased in comparison to the neighbouring regions near the axis. Now the dominant behaviour is a further growth of the pressure away from the axis. The pressure drop between the boundary of the collimated region and the z-axis is much higher than the pressure drop across shock (1). Therefore, at larger distances this pressure drop results in further compression of the flow toward the z-axis. To illustrate what happens at distances
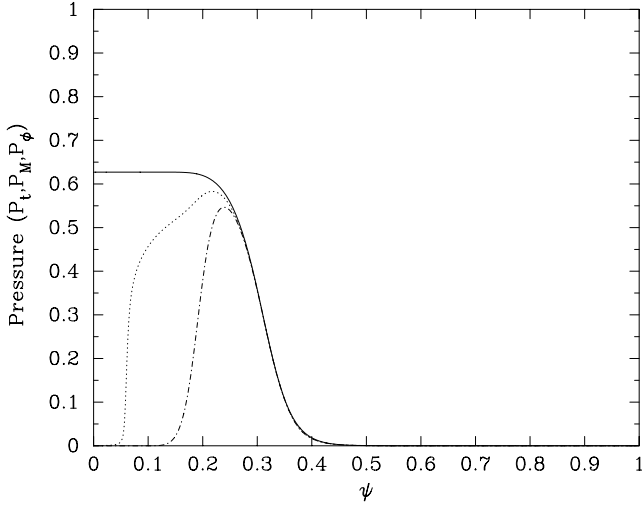
Figure 5. Distribution of total pressure $P_t = P + (B_p^2 + B_\varphi^2 - E^2)/8\pi$ (thermal + electromagnetic)(solid line), total electromagnetic pressure $P_M = (B_p^2 + B_\varphi^2 - E^2)/8\pi$ (dotted line) and pressure of toroidal field $P_\phi = (B_\varphi^2 - E^2)/8\pi$ (dash-dotted line) along a surface of constant η crossing the z-axis at $z = 10^5 \, R_f$.
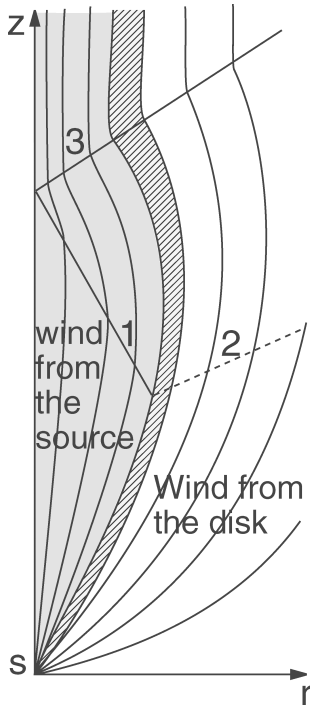
Figure 6. Sketch of the shock waves and singular surfaces expected to be formed in the general case of the collision of our two-component outflow. The oblique shock front marked by '1' is formed at the collision of the two parts of the exterior collimated and still uncollimated interior flows. An outgoing weak discontinuity from one end of this shock is marked by '2'. The shock front marked by '3' is formed at the self-reflection of the collimated flow by the axis of rotation.

exceeding $2000R_f$ we later plot in Fig. 10 the behaviour of the first 20 field lines (divided by the constant normalized flux equal to 10^{-3}). We see that after $2000R_f$ there is a small deflection of the flow from the z-axis and then the flow continues to move toward the z-axis,

because the pressure at the centre still remains small compared with the pressure of the compressing field. This may be seen in Fig. 9(a). Note also the oscillations in the jet's width in Fig. 10, as discussed analytically in Vlahakis & Tsinganos (1997).

At larger distances, $R \sim 20.000R_f$, the jet has been compressed to its minimum radius. The pressure distribution that corresponds to this moment is shown in Fig. 9(b). At this stage the overpressure of the flow at the axis produces the reflecting shock wave (3). This distribution of the pressure will now turn the flow off the z-axis. The reflecting shock wave (3) is easily seen at relatively large distances from the axis, because the amplitude of the reflecting shock grows as the magnetic pressure decreases. Here the effect is similar to what happens when a sound wave propagates in a region of decreasing density, wherein it is transformed into a shock wave (Zel'dovich & Raizer 2002). Indeed, at the beginning this distribution of the pressure creates a smooth motion of the plasma away from the z-axis. However, at larger distances where the total magnetic field decreases, this motion results in the formation of a reflecting shock wave, which corresponds to the predicted shock (3) in Fig. 6. The pressure distribution demonstrating the appearance of the reflected shock wave is shown in Fig. 9(c) where the shock is the discontinuity at about $\psi \leqslant 0.4$. Actually this reflection shock may also be seen in the general picture of Fig. 4.

Finally, it is interesting to examine for a moment the dependence of the temperature as a function of the coordinate z (Fig. 11a) because a temperature increase may result in observable phenomena. Although the plasma before the shock has a zero temperature, we see from this figure that in the post-shock region the gas is heated. A small finite temperature was produced at the first steps due to some unavoidable numerical errors in defining the initial surface and boundary conditions. Then, the temperature adiabatically drops with distance up to the distance when shock (1) has reached the z-axis (Fig. 8b). Here we see the first jump of the temperature. Then, the temperature adiabatically increases due to the compression by the outer toroidal magnetic field, and reaches a maximum value of $T \approx 0.8mc^2$ at the distance of $R \approx 20.000R_f$. This corresponds approximately to a temperature $T \approx 40\,\mathrm{keV}$ for an electron–positron plasma, or $T \approx 80\,\mathrm{MeV}$ for an electron–proton plasma.

In Fig. 11(b) the density of the plasma along the first 10 magnetic field lines near the axis is plotted as a function of z. The compression across the shock is by a factor of approximately 3. The velocity jump across the shock is also evident in Fig. 11(c), where for comparison the initial four-speed is shown by the dotted line. Because the shock is rather oblique and the outflow highly relativistic, the four-speed changes by a fraction of approximately 10 per cent.

In Fig. 12(a) we present the distribution of the poloidal four-velocity at the distance $z = 24\,000$ compared with the poloidal velocity distribution at the base. Note first that at large $\psi > 0.3$ there is an acceleration of the plasma, although at smaller ψ the poloidal velocity is smaller than the initial one. To understand this behaviour, we recall that the steady MHD equations admit four integrals:

(α) the ratio of the poloidal magnetic and mass fluxes, $cF(\psi)$

$$cF(\psi) = B_p/4\pi\rho v_p; \tag{8}$$

(β) the total angular momentum per unit mass, $L(\psi)$

$$x\omega U_\varphi - Fx\omega B_\varphi = \frac{\Omega(\psi)L(\psi)}{c^2}; \tag{9}$$
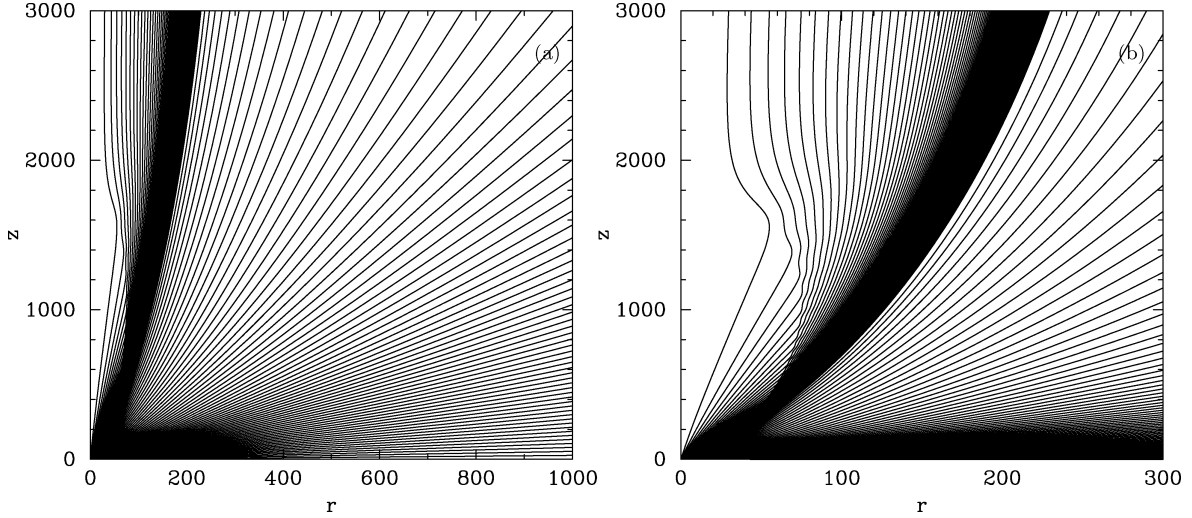
Figure 7. (a) A detailed view of the flow up to $z = 3000R_f$ is shown. Note that the scale on the horizontal axis r is three times larger than that in the z-axis. The plotting of the magnetic flux between field lines after $\psi > 0.3$ is less dense by a factor of 10. A magnification of this plot is shown in (b).
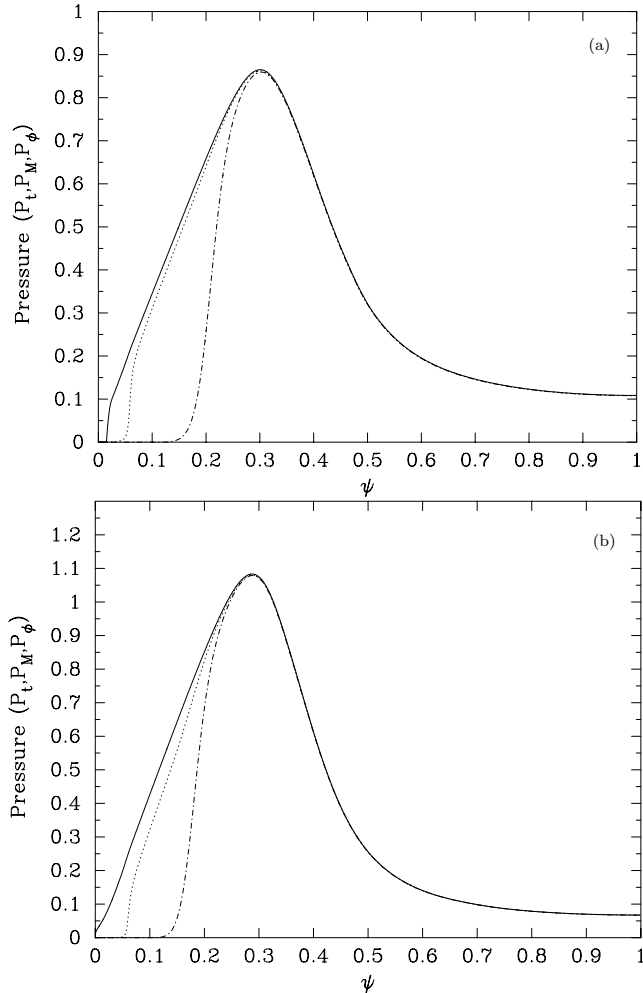
Figure 8. Distribution of the pressures along a surface of constant η which crosses the z-axis at $412R_f$ and $2141R_f$. Note that in (b) the pressure in the post-shock region is already of thermal origin. All the notations are similar to those in Fig. 5.

(γ) the corotation frequency $\Omega(\psi)$ in the frozen-in MHD condition

$$U_\varphi B_p - U_p B_\varphi = \Gamma x \omega(\psi) B_p; \tag{10}$$

(δ) finally the total energy $W(\psi)$ in the equation for total energy conservation

$$\Gamma - F x \omega B_\varphi = W(\psi). \tag{11}$$

Here, $\Gamma = \gamma (e + p)$. By combining equations (9) and (11) we have

$$\Gamma - x U_\varphi = W(\psi) - \frac{\Omega(\psi)L(\psi)}{c^2}. \tag{12}$$

In the region where the toroidal velocity is positive (negative) (see Fig. 12b) the plasma is accelerated (decelerated) because the Lorentz factor increases (decreases). Thus, along a constant ψ a reduction of the toroidal velocity leads to a reduction of the energy of the plasma. The deceleration just at the rotational axis is explained by another reasoning. At the axis, Γ is an integral and does not vary with distance. The decrease of U_p is due to the heating of the plasma because of the shock. At the axis, the Lorentz factor and the poloidal velocity are related as

$$\Gamma^2 = U_p^2 + (e + p)^2. \tag{13}$$

The increase of the plasma temperature results in an increase of the $e + p$ term. Then, U_p should eventually decrease, because Γ is constant.

To demonstrate the role of the toroidal component of the velocity in the formation of the jet structure we plotted the distribution of the toroidal four-velocity U_φ versus ψ in Fig. 12b, together with the normalized distribution of the angular velocity. The angular velocity of the field line rotation is positive everywhere. Nevertheless, on some of the field lines the plasma rotates in the opposite direction. This result is due to the compression of the flow by the disc-wind wherein the poloidal magnetic field increases. Then, it follows that the poloidal Alfvén number decreases, and subsequently the toroidal magnetic field increases because in MHD it depends inversely on the poloidal Alfvén Mach number. In the expression for the conserved total angular momentum, an increase of the azimuthal magnetic field is accompanied by a decrease of the toroidal velocity. Because in the inner regions the toroidal speed was initially zero, this means
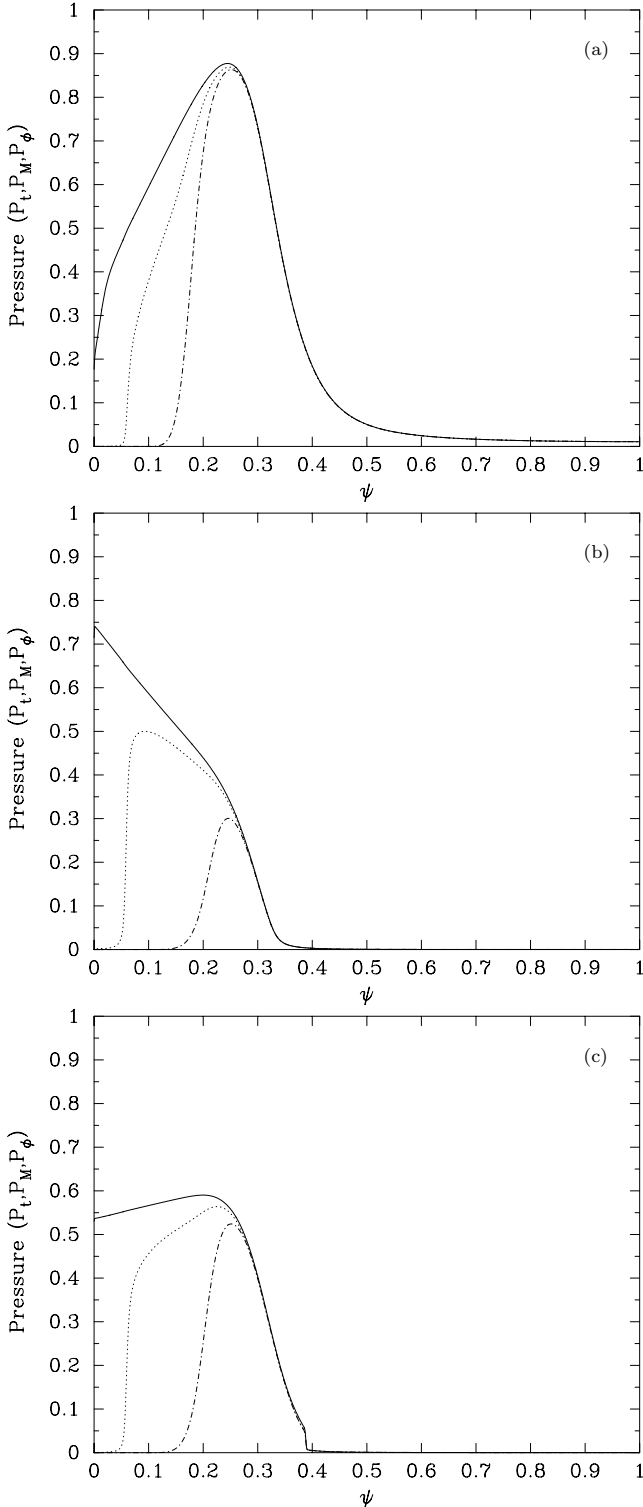
Figure 9. Pressure distribution on a surface of constant η crossing the z-axis at the distance $11\,000R_f$ in (a), at $20.000R_f$ where the pressure at the z-axis obtains a maximum value and the jet reaches its minimum radius in (b), and at $24.000R_f$ in (c). In (c), note that close to $\psi = 0.4$ the reflecting shock front moving towards the direction of large ψ may be seen.

that it becomes negative. We should add that the toroidal velocity is very small and does not affect the formation of the jets.

5 CONCLUSION

By using a simplified model and an efficient numerical scheme, in this paper we have demonstrated that all relativistic mass flux from a central source can be collimated, provided that the outflow in addition to the initially uncollimated relativistic plasma component from the central source possesses a second component of a non-relativistic wind from the surrounding disc, which plays the role of the flow collimator. The magnetic and mass flux from the central source of the relativistic outflow was about 30 per cent of the total flux from our system. It is important that 100 per cent of the flux from the central source has been collimated into a relativistic jet. During the collimation of the inner relativistic flow, collision and reflection shocks were formed.

A preliminary calculation of the collimation process in conditions appropriate to specific astrophysical objects has been performed for the case of the M87 jet, wherein it is found that this relativistic jet collimates from a wide opening angle of about 60° at subparsec scales to a smaller angle of about 10° at the parsec scale, in agreement with observations (Tsinganos & Bogovalov 2004). Here our purpose was restricted to resolving the difficulty of the theory of magnetic collimation to form jets with a large fraction of the total mass flux of the outflow from the central source. We succeeded in obtaining this rather interesting result, by using an admittedly simplified and crude model. Another by-product of this work is that some important processes accompanying the collimation of astrophysical plasmas, such as the formation of shocks, occur in the supersonic, or MHD super-fast region. A shortcoming of the present study, as far as a direct application of the results to jet formation in specific astrophysical objects is concerned, is that some additional physical ingredients (thermal pressure, non-zero angular velocity of rotation of the central source, etc.) have not been included in the present modelling, something which will be the next step in this study (e.g. Tsinganos & Bogovalov 2004). Work is in progress for one of the final steps of this project, namely a direct connection of this shock formation to particle acceleration and radiation emission in order to directly relate the results of the present model to the observed radiation patterns from relativistic jets.

Besides the analytical studies using self-similarity (Tsinganos et al. 2004), several other numerical simulations of the astrophysical jet phenomenon have been performed, as noted in the Section 1. Recently, Zanni et al. (2004) used high-resolution MHD simulations with adaptive mesh refinement to examine the acceleration and collimation of jets from an accretion disc. After following the system for several rotations of the inner part of the disc, a growing mass outflow rate in the jet was found, but the system did not reach equilibrium. As far as the question of the stability of the solution is concerned, we note that a full examination of the stability of jets is still an open problem (see Ouyed, Clarke & Pudritz 2003). As for the numerical stability of our solution, we found no signature of numerical instability by exploring the solution parameter space.
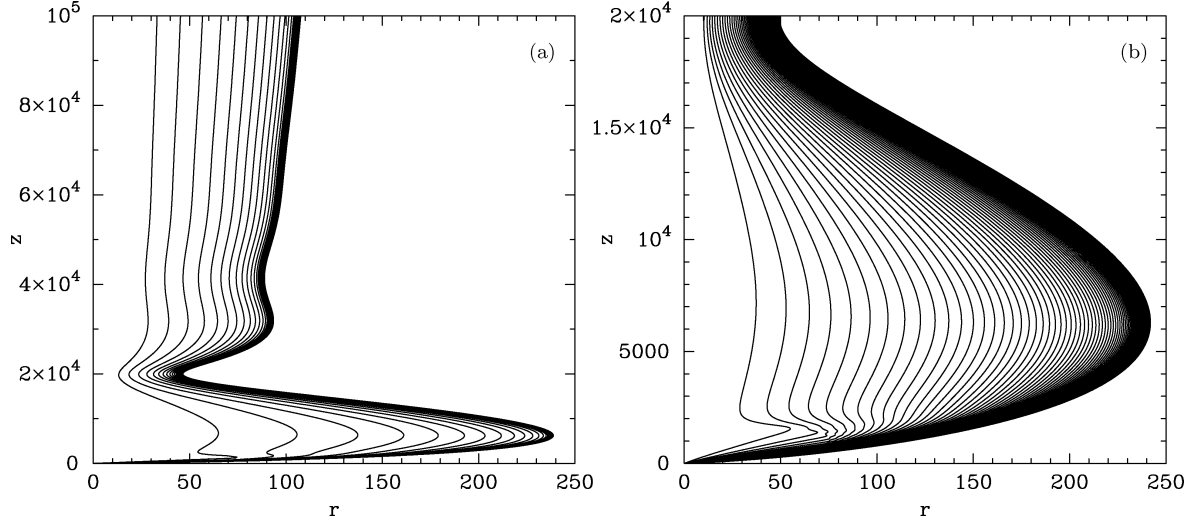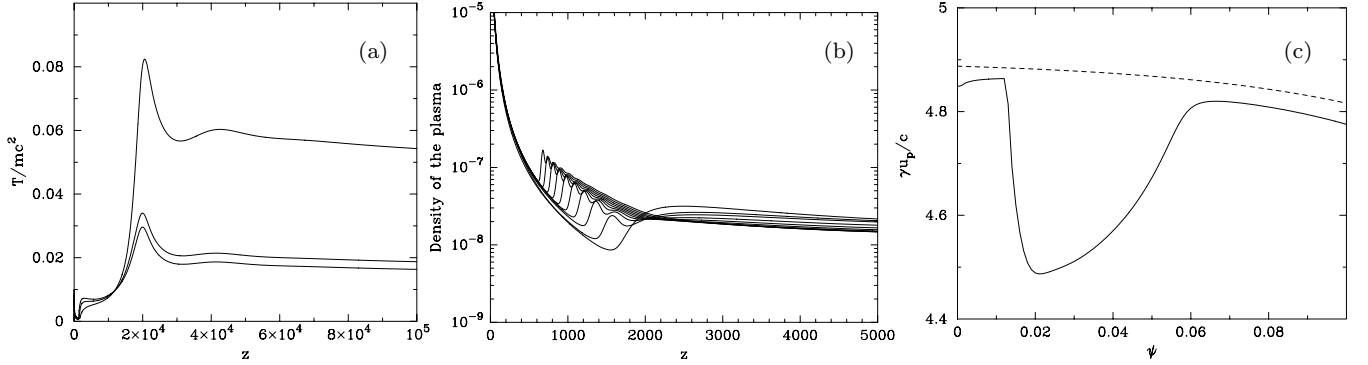
Figure 10. (a) The magnetic field lines are plotted in intervals of 4 over the original field to clearly show the compression of the central outflow to form a jet with an oscillatory radius. A magnification of (a) is shown in (b) where all field lines are plotted.

Figure 11. In the left panel is shown the dependence of the temperature in the first three field lines as a function of the distance z, with the upper curve corresponding to the temperature at the z-axis. In the middle panel is shown the density distribution of the plasma along the first 10 magnetic field lines near the axis plotted as a function of z. Finally, in the right panel is shown the velocity jump across the shock as a function of the magnetic flux ψ, at the distance $500 R_f$. For comparison, the initial four-speed is shown with the dotted line.
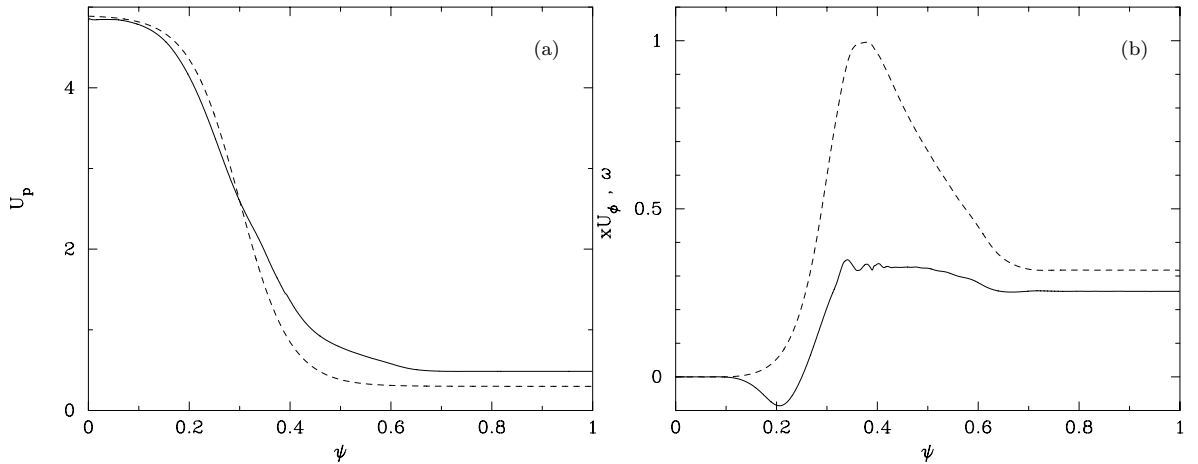
Figure 12. At $z = 24\,000$ as a function of ψ are shown, in the left panel, the distributions of the final (solid line) and initial (dashed line) poloidal plasma four-speeds U_p. In the right panel the final azimuthal plasma four-speed xU_ϕ after the evolution of the system (solid line) is shown together with the initial angular rotation frequency ω (dashed line).

REFERENCES

Biretta J. A., Junor W., Livio M., 2002, New Astron. Rev., 46, 239
Biretta J. A., Sparks W. B., Macchetto F., 1999, ApJ, 520, 621
Bisnovatyi-Kogan G., Ruzmaikin A. A., 1976, Astrophys. Space. Sci., 42, 401
Blandford R. D., 1976, MNRAS, 176, 465
Bogovalov S. V., 1995, Sov. Astron. Lett., 21, 4
Bogovalov S. V., Tsinganos K., 1999, MNRAS, 305, 211 (BT99)
Chiueh T., Li Z.-Y., Begelman M. C., 1991, ApJ, 377, 462
Cramphorn C. K., Sazonov S. Yu., Sunyaev R. A., 2004, A&A, 420, 33
Ferrari A., 1998, ARA&A, 36, 539
Ferreira J., Pelletier G., Apple S., 2000, MNRAS, 312, 387
Gabuzda D. C., Eammon M., Cronin P., 2004, MNRAS, 351, L89
Godunov S. K., 1959, Math. Sborniak, 89(47), 271
Gracia J., Peitz J., Keller Ch., Camenzind M., 2003, MNRAS, 344, 468
Heyvaerts J., Norman C. A., 1989, ApJ, 347, 1055
Heyvaerts J., Norman C. A., 2003, ApJ, 596, 1270
Krasnopolsky R., Li Z.-Y., Blandford R., 1999, ApJ, 526, 631
Krasnopolsky R., Li Z.-Y., Blandford R., 2003, ApJ, 595, 631
Kudoh T., Matsumoto R., Shibata K., 1998, ApJ, 508, 186
Landau L. D., Lifshitz E. M., 1959, Fluid Mechanics. Pergamon Press, Oxford
Livio M., 1999, Phys. Rep., 311, 225
Lovelace R. V. E., 1976, Nat, 262, 649
Mirabel F. C., Rodríguez L. F., 1999, ARA&A, 37, 409
Ouyed R., Pudritz R. E., 1997, ApJ, 484, 794
Ouyed R., Clarke D. A., Pudritz R. E., 2003, ApJ, 582, 292
Pelletier G., Fereira J., Henri G., Marcowith A., 1996, in Tsinganos K., ed., Solar and Astrophysical MHD Flows. Kluwer Academic, Dordrecht, p. 643
Sauty C., Tsinganos K., 1994, A&A, 287, 893
Shakura N. I., Sunayev R. A., 1973, A&A, 24, 337
Sol H., Pelletier G., Asseo E., 1989, MNRAS, 237, 411
Spruit H. C., 1994, in Lynden-Bell D., ed., Cosmical Magnetism. Kluwer, Dordrecht, p. 33
Tsinganos K., Bogovalov S. V., 2000, A&A, 356, 989 (TB00)
Tsinganos K., Bogovalov S. V., 2002, MNRAS, 337, 553 (TB02)
Tsinganos K., Bogovalov S. V., 2005, in Aharonian F. A., Volk H., eds, High Energy Gamma-ray Astronomy. Am. Inst. Phys., New York, in press
Tsinganos K., Vlahakis N., Bogovalov S. V., Sauty C., Trussoni E., 2004, Ap&SS, 293, 55
Ustyugova G. V., Koldoba A. V., Romanova M. M., Chechetkin V. M., Lovelace R. V. E., 1999, ApJ, 516, 221
van Leer B., 1977, J. Comput. Phys., 23, 276
Vlahakis N., Tsinganos K., 1997, MNRAS, 292, 591
Vlahakis N., Tsinganos K., 1998, MNRAS, 298, 777
Vlahakis N., Tsinganos K., 1999, MNRAS, 307, 279
Vlahakis N., Tsinganos K., Sauty C., Trussoni E., 2000, MNRAS, 318, 417
Zanni C., Ferrari A., Massaglia S., Bodo G., Rossi P., 2004, Ap&SS, 293, 99
Zel'dovich Ya. B., Raizer Yu. P., 2002, Physics of Shock Waves and High-temperature Hydrodynamic Phenomena. Dover, New York

APPENDIX A: HD OBLIQUE RELATIVISTIC SHOCKS

For the demonstration of the ability of our code to reproduce the correct jump conditions of oblique relativistic shocks, we present the test results of the simulation of a uniform supersonic plasma flow incident on a tube with a broken wall. At the break the incident plasma flow with $U_1 = 5$ is turned at an angle $\delta = 5°$. The flow

line near the wall is shown in Fig. A1 wherein all notations are also shown. In the limit of high temperature $T \gg mc^2$ and for the relativistic relationship between the energy density and pressure, $e = 3p$, the relationship between the angles is obtained as follows (see Landau & Lifshitz 1959). First, in the above ultrarelativistic limit the equations giving the pre-shock and post-shock velocities are

$$\left(\frac{v_1}{c}\right)^2 = \frac{1}{3}\frac{3p_2 + p_1}{3p_1 + p_2}, \qquad \left(\frac{v_2}{c}\right)^2 = \frac{1}{3}\frac{3p_1 + p_2}{3p_2 + p_1}, \tag{A1}$$

where v_1 (v_2) is the magnitude of the velocity of the pre-shocked (post-shocked) plasma in a coordinate system where the plasma velocity along the shock front is equal to zero. It follows from these equations that the normal component of the initial four-velocity ($U = \gamma v/c$) is

$$U_{1,\perp}^2 = \frac{3p_2 + p_1}{8p_1}. \tag{A2}$$

This normal component of the four-velocity is invariant in relation to Lorentz transformations corresponding to a motion along the shock front. Therefore, in the laboratory system and if the flow makes an angle ϕ with the plane of the shock, the incident flow component normally to the shock is $U_{1,\perp} = U_1 \sin \varphi$ (see Fig. A2). From this we obtain the ratio of post-shock/pre-shock pressures:

$$\frac{p_2}{p_1} = \frac{8U_1^2 \sin^2 \varphi - 1}{3}. \tag{A3}$$

The value of the pressure jump at the shock can also be obtained in another way. The energy momentum conservation equation $\partial T_i^k / \partial x^k = 0$ can be written in an integral form

$$\sum_l T_i^k S_k^l e^i = 0. \tag{A4}$$

Here the summation on l is performed over all the surface patches surrounding the volume, e is a unit vector and S denote the vectors normal to the surface and proportional to the surface area. Let us take the integration volume and vector e as shown in Fig. A2. In this case from equation (17) it follows that
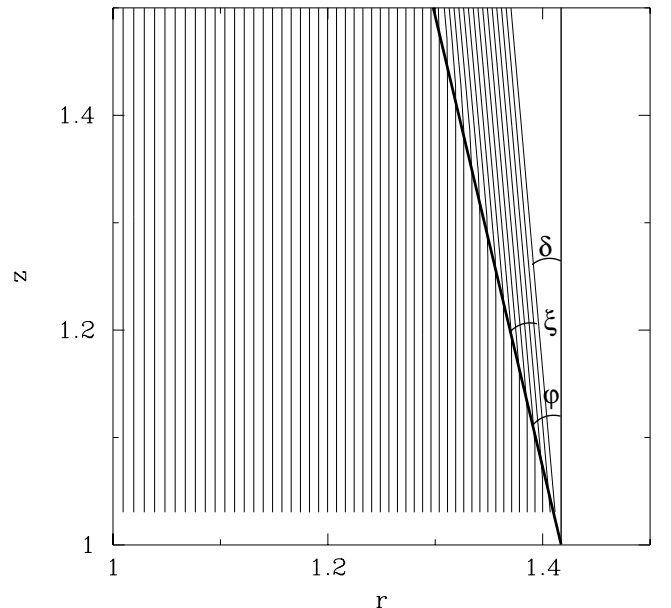
Figure A1. The flow lines at the wall with a break. The break angle is taken to be 5°.
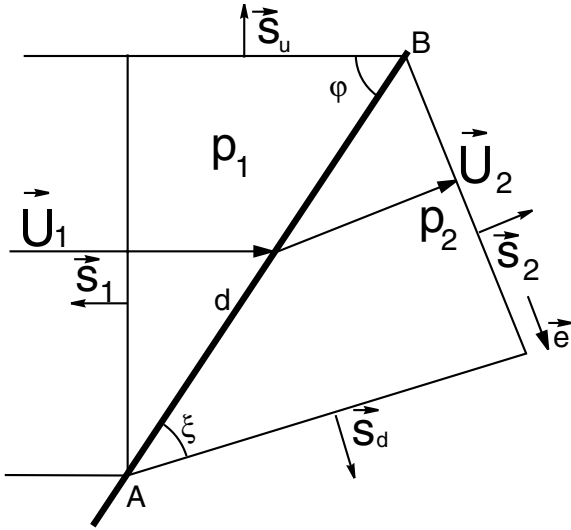
Figure A2. The volume of integration is formed by the stream lines with normal surface vectors S_u and S_d and by the surfaces S_1 and S_2 normal to the stream lines. The plasma in the pre-shock region is marked by the index '1' and in the post-shock region by the index '2'. The shock front is the thick line AB.

$$-w_1(U_1 S_1) \ U_1 \cos[90 - (\varphi - \xi)] - p_1 S_1 \cos[90 - (\varphi - \xi)]$$
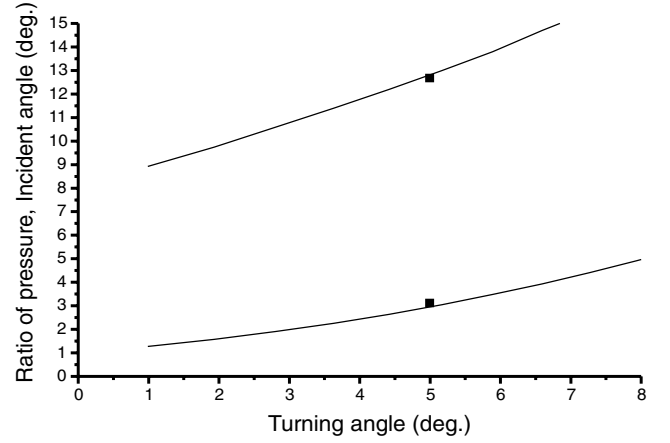$$- p_1 S_u \cos(\varphi - \xi) + p_2 S_d = 0. \tag{A5}$$

By taking $S = 1$, we have $S_u = \cos\varphi$ and $S_d = \sin\xi$ such that the above relation becomes

$$w_1 U_1^2 \sin(\varphi - \xi) \ \sin\varphi + p_1 \sin(\varphi - \xi) \sin\varphi$$
$$+ p_1 \cos(\varphi - \xi) \cos\phi = p_2 \cos\xi, \tag{A6}$$

or

$$w_1 U_1^2 \sin\delta \sin\phi + p_1 \cos\xi = p_2 \cos\xi, \tag{A7}$$

where $\delta = \varphi - \xi$. Substituting $w = 4p$ we have

Figure A3. The ratio of the pressure upstream and downstream of the shock (lower curve) and dependence of φ on δ (upper curve). Squares indicate the values obtained in the numerical solution for $U_1 = 5$.

$$\frac{p_2}{p_1} = 1 + 4U_1^2 \frac{\sin\varphi \sin\delta}{\cos\xi}. \tag{A8}$$

Finally, combining equations (A3) and (A8) we obtain

$$\tan\xi = \frac{1}{3}\tan\varphi + \frac{1}{3\cos\varphi \sin\varphi U_1^2}. \tag{A9}$$

In other words, equation (A9) relates the angle φ between the shock front and the incident flow with the turning angle δ, while equation (A8) relates the ratio of the pressures at the two sides of the shock with δ. This dependence of the angle φ and ratio of pressure upstream (P_1) and downstream (P_2) of the shock on δ is shown in Fig. A3.

This paper has been typeset from a TEX/LATEX file prepared by the author.